






ARTICLE

DOI: 10.1038/s41467-018-05757-6

OPEN

Interfacing with silica boosts the catalysis of copper

Chaofa Xu ¹, Guangxu Chen¹, Yun Zhao¹, Pengxin Liu¹, Xinping Duan ¹, Lin Gu ²,
Gang Fu¹, Youzhu Yuan ¹ & Nanfeng Zheng ¹

Metal-support interaction is one of the most important parameters in controlling the catalysis of supported metal catalysts. Silica, a widely used oxide support, has been rarely reported as an effective support to create active metal-support interfaces for promoting catalysis. In this work, by coating Cu microparticles with mesoporous SiO₂, we discover that Cu/SiO₂ interface creates an exceptional effect to promote catalytic hydrogenation of esters. Both computational and experimental studies reveal that Cu-H^{δ-} and SiO-H^{δ+} species would be formed at the Cu-O-SiO_x interface upon H₂ dissociation, thus promoting the ester hydrogenation by stabilizing the transition states. Based on the proposed catalytic mechanism, encapsulating copper phyllosilicate nanotubes with mesoporous silica followed by hydrogen reduction is developed as an effective method to create a practical Cu nanocatalyst with abundant Cu-O-SiO_x interfaces. The catalyst exhibits the best performance in the hydrogenation of dimethyl oxalate to ethylene glycol among all reported Cu catalysts.

¹State Key Laboratory for Physical Chemistry of Solid Surfaces, Collaborative Innovation Center of Chemistry for Energy Materials, National & Local Joint Engineering Research Center for Preparation Technology of Nanomaterials, and National Engineering Laboratory for Green Chemical Productions of Alcohols-Ethers-Esters, College of Chemistry and Chemical Engineering, Xiamen University, Xiamen 361005, China. ²Institute of Physics, Chinese Academy of Sciences, Beijing 100190, China. These authors contributed equally: Chaofa Xu, Guangxu Chen. Correspondence and requests for materials should be addressed to G.F. (email: gfu@xmu.edu.cn) or to Y.Y. (email: yzyuan@xmu.edu.cn) or to N.Z. (email: nfzheng@xmu.edu.cn)

Heterogeneous catalysis is of vital importance in many fields of chemical, food, energy, and environmental applications. The rational design and fabrication of sufficient active interfaces between metal and (hydr)oxide to facilitate the reactions with multiple reagents has emerged as an effective strategy to prepare heterogeneous catalysts with improved performances. For instance, both Pt/FeO_x and Pt/Fe(OH)_x interfaces exhibit excellent performance in CO oxidation and CO preferential oxidation (PROX)^{1–4}. Au/CeO_x and Au/TiO_x interfaces have been demonstrated to improve the activity of water-gas shift reaction^{5–7}. Pt/M(OH)₂ (M = metal) interfaces enhance the performance of hydrogen evolution reaction and hydrogen oxidation reaction^{8–11}. Such interfacial effects from the strong metal–metal (hydr)oxide interactions were typically observed only when reducible metal oxides (e.g., TiO_x, CeO_x, FeO_x) were used as supports^{12–17}. In contrast, SiO₂ without reducible metal cations usually serves as ‘inert’ support, or plays as shell material to fabricate yolk-shell and core-shell metal nanocatalysts to prevent the sintering of metal components^{18–24}. Reports on the promotional effects of SiO₂ on heterogeneous catalysis are rare^{25,26}.

Here we demonstrate that SiO₂ readily creates highly active interfaces with Cu in the gas-phase hydrogenation of dimethyl oxalate (DMO) into ethylene glycol (EG). In this work, the Cu–SiO₂ interfaces were first designed and fabricated by depositing a mesoporous SiO₂ (m-SiO₂) layer onto the surface of commercial Cu powders. With the created Cu–SiO₂ interfaces, the coated Cu powders exhibited a two-order-of-magnitude enhancement in the activity as compared to the uncoated Cu powders. Combining experiments with density functional theory (DFT) calculations, we demonstrate that H₂ could be activated at the Cu^{δ+}–O–SiO_x interface region, giving rise to Cu–H and interfacial SiO–H species, which are able to promote the hydrogenation of polar C=O bonds. Based on this understanding, a smart strategy by *in situ* reducing silica coated copper phyllosilicate nanotubes was developed to produce a sophisticated Cu–SiO₂ nanocatalyst with abundant Cu–O–SiO_x interface. Such a catalyst exhibited the best reported performance in selective hydrogenation of DMO to EG.

Results and Discussion

Cu–O–SiO_x interfaces boost the catalysis of copper. To create Cu–O–SiO_x interfaces, a non-continuous layer of m-SiO₂ was deposited onto the surface of commercial Cu microparticles (MPs) with diameter of 2–3 μm by hydrolysis of tetraethoxysilane (TEOS) in the presence of cetyltrimethylammonium bromide (CTAB) (See ‘Methods’ section). Scanning electron microscopy (SEM) and energy dispersive spectroscopy (EDS) analysis (Fig. 1a–h, Supplementary Fig. 1) revealed the successful deposition of a downy layer of SiO₂ on Cu MPs. The mesoporous nature of the SiO₂ layer deposited on Cu MPs was confirmed by the N₂ adsorption and desorption isotherm at 77 K (Supplementary Fig. 2). It should also be noted that the m-SiO₂ layer was not continuously grown on Cu, resulting in the exposure of partial Cu sites on the as-obtained hybrid of Cu-MP@m-SiO₂.

To evaluate the Cu–O–SiO_x interfacial effect, we chose the gas-phase hydrogenation of DMO.^{27–29} As shown in Fig. 1i, Cu MPs without SiO₂ coating displayed a negligible activity in the hydrogenation of DMO at the temperature below 250 °C. In comparison, Cu MPs coated with m-SiO₂ exhibited a significant activity even at the temperature of 210 °C. The turnover rate of carbonyl groups ($k_{\text{carbonyl group}}$) over Cu-MP@m-SiO₂ was approximately 80 times higher than that on uncoated Cu MPs at the temperature between 200 and 240 °C. In this comparison, the $k_{\text{carbonyl group}}$ was calculated based on the hydrogenation rate of carbonyl groups over the total amount of Cu in the catalysts.

The hydrogenation activity of the Cu-MP@m-SiO₂ catalyst was increased with the temperature. Considering that less Cu sites were exposed on Cu-MP@m-SiO₂, the catalytic enhancement induced by the Cu–O–SiO_x interfaces was tremendous. Moreover, the apparent activation energy (E_a) over Cu-MP@m-SiO₂ was measured to be 107.1 kJ mol^{–1} (Fig. 1j), almost only half of that on Cu MPs (188.9 kJ mol^{–1}), indicating the as-built Cu–O–SiO_x interfaces would completely alter the hydrogenation mechanism.

Hydrogenation mechanism over the Cu–O–SiO_x interface. The promotional effect of the Cu–O–SiO_x interface on the catalytic hydrogenation of DMO was studied by using DFT calculations. In this work, structural models of periodic Cu(111) with/without SiO₂ coating were built to simulate the modified and unmodified Cu MPs, respectively. Until now, it is still a great challenge to identify the interfacial structure between metal and silica since the SiO₂ deposition could present as various crystalline or vitreous films. To simplify the interface model, we assumed that the [SiO₄] tetrahedra could be stacked on Cu(111) in a two-dimensional ordered network with a composition of SiO_{2.5}, in which every Si has one Si–O–Cu bond and three Si–O–Si bonds (Supplementary Fig. 3). According to our DFT calculations, the proposed model was calculated to be exothermic by 0.66 eV/Si with respect to Cu(111), α-quartz SiO₂ and gaseous O₂. Bader charge analysis showed that surface Cu atoms, which were directly bonded with O–SiO₃, would carry significantly positive charge, implying that the SiO₂ overgrowth would lead to the formation of Cu^{δ+} species (Supplementary Fig. 3). Interestingly, similar silica films with c(2 × 2) structures have been demonstrated to form on Mo(112) and Ru(0001) single crystal surfaces^{30–32}. As suggested previously, the adsorption energy of oxygen atoms plays an important role in determining whether silica monolayer film can be stabilized on the metal surface or not. In our case, the dissociative adsorption energy of O₂ on Cu(111) was calculated as –3.13 eV, just between those of Mo(112) (–5.64 eV) and Ru(0001) (–2.28 eV). In addition, Cu(111) has lattice constant of 2.556 Å, matching well with the silica film with a 5.2–5.3 Å periodicity in the (2 × 2) manner. All these results indicated that the formation of monolayer SiO₂ network over Cu(111) surfaces is reasonable. On the surface of Cu-MP@m-SiO₂, there were still a large amount of uncovered Cu atoms so that the silica film should not be continuous. To account for the experimental observation, we extended our model to a (8 × 4) structure in which 50% [SiO₄] tetrahedra were removed, and the as-generated Si–O dangling bonds were saturated by H atoms. Thus, the Cu–O–SiO_x interface turned to be accessible for the substrate molecules. Hereafter, such a model is denoted as SiO₂/Cu(111).

Hydrogenation on the heterogeneous catalysts usually follows Horiuti Polanyi mechanism, which consists of following steps: (i) dissociation of hydrogen; (ii) adsorption of unsaturated compounds; (iii) stepwise hydrogenation with H atoms. Supplementary Fig. 4 showed the dissociation of H₂ on the two distinct surfaces, i.e., Cu(111) and SiO₂/Cu(111). On Cu(111), H–H bond splitting occurred via a homolytic mechanism, generating two hydrogen atoms adsorbed on the three-fold sites. Alternatively, the presence of Cu–O–SiO_x interface on SiO₂/Cu(111) enable H₂ activation in a heterolytic way, yielding Cu–H and interfacial SiO–H species simultaneously at the interface. From Cu(111) to SiO₂/Cu(111), the calculated barrier for H₂ dissociation does not change too much (0.28 eV vs. 0.30 eV), indicating that heterolytic dissociation could be competitive with the homolytic one. However, from the viewpoint of thermodynamics, H₂ dissociation on SiO₂/Cu(111) was found to be more exothermic than that on Cu(111) (–0.81 eV vs. –0.47 eV) because the interfacial SiO–H bond is stronger than Cu–H bond. Therefore, even the H₂

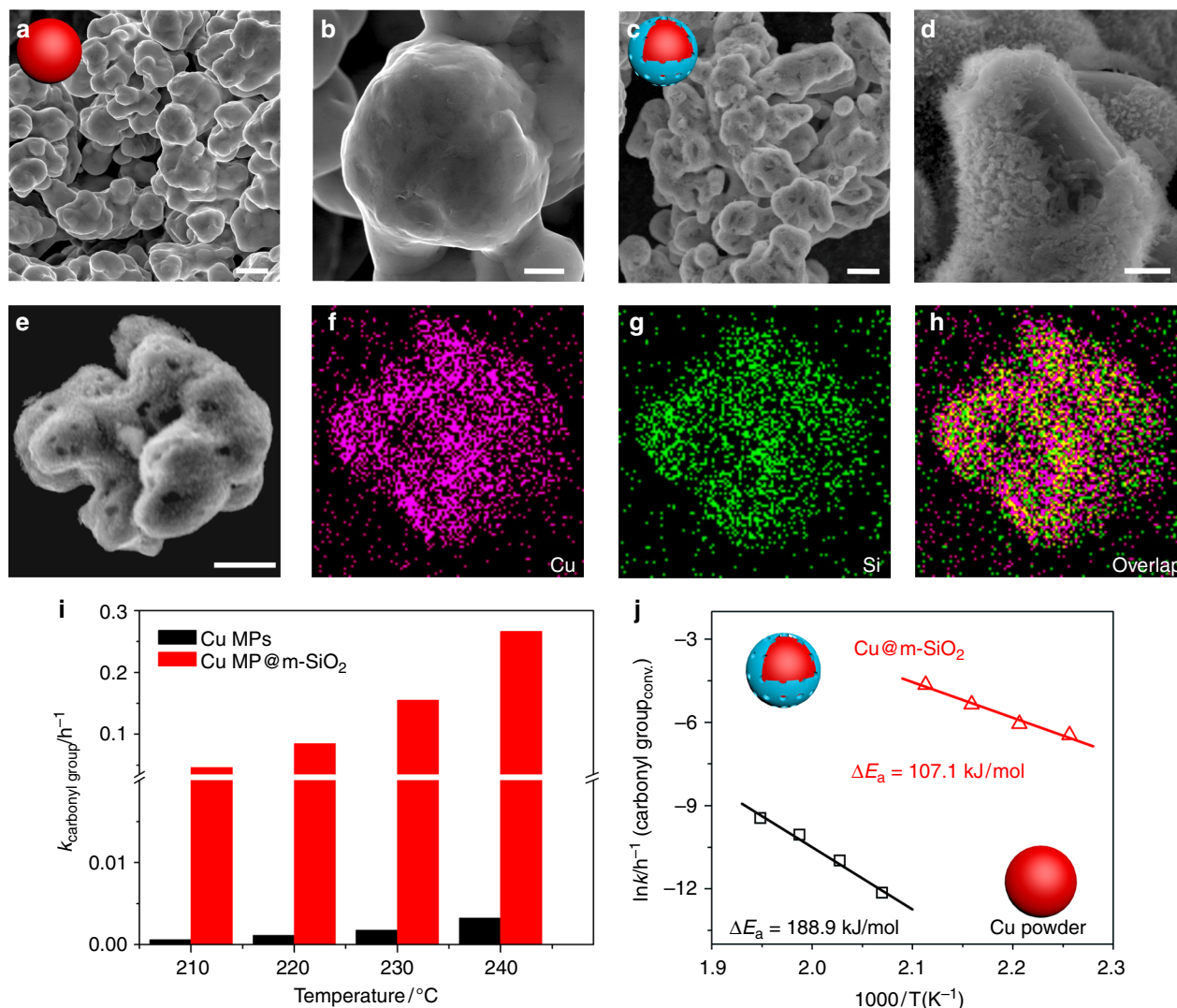


Fig. 1 Demonstration of Cu–O–SiO_x interface effect in DMO hydrogenation. **a–d** SEM images of Cu microparticle before (**a, b**) and after (**c, d**) coating mesoporous silica; **e–h** EDX mapping images of mesoporous silica coated Cu microparticles (Cu@m-SiO₂); **i, j** Catalytic performance and the apparent activation energy (E_a) of Cu microparticles before and after coating mesoporous silica for the selective hydrogenation of DMO, respectively; Reaction conditions were as follows: $\text{H}_2/\text{DMO} = 80 \text{ mol/mol}$, $P(\text{H}_2) = 3.0 \text{ MPa}$. Scale bars in **a, c** and **e** are 2 μm . Scale bars in **b** and **d** are 500 nm

dissociation occurred via the hemolytic route, interfacial $\text{SiO}-\text{H}^{\delta+}$ species would be generated through thermodynamics-driven hydrogen spillover. All these indicated that there existed abundant interfacial $\text{SiO}-\text{H}^{\delta+}$ and $\text{Cu}-\text{H}^{\delta-}$ at the Cu–O–SiO_x interfaces upon hydrogenation.

The DMO hydrogenation pathways on Cu(111) and SiO₂/Cu(111) were compared, with the optimized structures of transition states (TS) and important intermediates (IMs) illustrated in Fig. 2a, Supplementary Figs. 5 and 6. For clarity, only the lowest energy pathways were shown for these two surfaces. According to our DFT calculations, DMO was weakly adsorbed on both Cu(111) and SiO₂/Cu(111) (from i to ii in Fig. 2a). In this regard, there are two possible mechanisms, namely hydroxyl mechanism and alkoxy mechanism. In the former case, the first hydrogen atom would attack the O end of C=O group, producing the hydroxyl intermediate, while in the latter case, C end of C=O group would be hydrogenated first, leading to the formation of alkoxy intermediate. It has been reported previously that hydroxyl intermediate was thermodynamically less favorable than alkoxy intermediate^{33,34}. On both surfaces, the hydrogenation of DMO begins with the nucleophilic attack of $\text{H}^{\delta-}$ to the

electron deficient carbon of ester group. On Cu(111), a 1.22 eV barrier (TS1) has to be surmounted when the initial hydrogenation takes place. In contrast, a relative low barrier of 0.77 eV (TS1) is required when the reaction occur at the Cu–O–SiO_x interface. It should be noted that both of the reactions proceed with similar endothermicity of $\sim 0.10 \text{ eV}$, indicating that the difference in the barrier should be attributed to the electronic effect (from ii to iii in Fig. 2a). Based on the Bader charge analysis, it was found that when $\text{H}^{\delta-}$ approaches, the adsorbed DMO would bear a $\sim -0.5 \text{ a.u.}$ charge. Such a negatively charged TS can be stabilized by the $\text{SiO}-\text{H}^{\delta+}$ species, but repulsive with the co-adsorbed $\text{Cu}-\text{H}^{\delta-}$. This finding nicely explained why the addition of ‘inert’ silica could significantly enhance the hydrogenation.

Next, the half-hydrogenated intermediate undergoes the second H addition to give alcohol species (iv in Fig. 2a IM2). On Cu(111), the TS2 occurs through a reductive elimination of $\text{CH}_3\text{O}(\text{O}=\text{C})-\text{CH}(\text{OCH}_3)\text{O}^{\delta-}$ and $\text{H}^{\delta-}$, yielding a barrier of 1.07 eV. Such a high barrier might be originated from the electrostatic repulsion between two negatively charged species. On the contrary, $\text{SiO}-\text{H}^{\delta+}$ at the Cu–O–SiO_x interface can

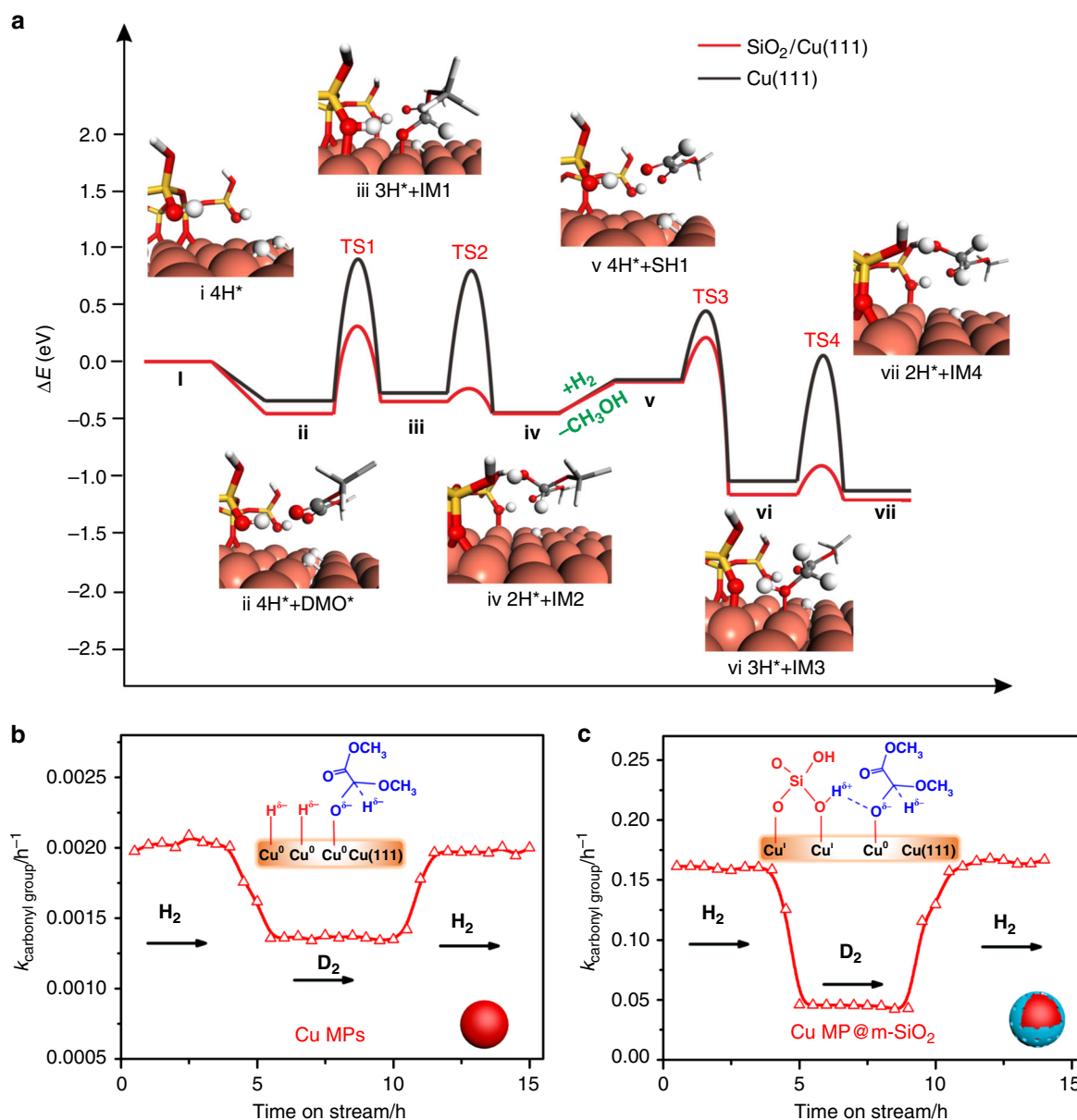


Fig. 2 Mechanism of DMO hydrogenation on Cu–O–SiO_x interface. **a** The DMO hydrogenation pathway on Cu(111) and SiO₂/Cu(111); **b, c** The kinetic isotope effect of Cu MPs catalyst and Cu MPs@m-SiO₂ catalyst in hydrogenation of DMO. Reaction conditions were as follows: H₂/DMO = 80 mol/mol, P (H₂) = 3.0 MPa, T = 230 °C

provide a proton, which is quickly transferred to CH₃O(O=)C–CH(OCH₃)O^{δ−} to make a O–H bond by passing a small barrier of 0.11 eV (from iii to iv in Fig. 2a). From this result, the interfacial SiO–H^{δ+} species should be very acidic since the Cu atoms at the interface can stabilize their deprotonated forms. The proposed mechanism nicely explains why the Cu–O–SiO_x interface is a good choice for the hydrogenation reaction. On one hand, the Cu–OSi bond is not so strong to inhibit the dissociation of H₂. On the other hand, moderate Cu–OSi bond would render interfacial SiO–H bond suitable strength, which not only stabilizes the charged TS' but also releases a proton when necessary.

For IM2, the co-presence of OH and OMe groups on the same carbon atoms makes them unstable, which can be easily converted into adsorbed CH₃O(O=)C–CHO (SH1) plus a methanol molecule (from iv to v in Fig. 2a). Subsequently, SH1 would undergo step-wise hydrogenation again, passing through

TS3 and TS4, leading to formation of MG species (IM4). Again, the calculated barriers for TS3 and TS4 on SiO₂/Cu(111) were much lower than those on Cu(111), and the hydrogenation of aldehyde groups was easier than that of the ester groups (from v to vii in Fig. 2a). Similarly, MG can further be hydrogenated into EG by consecutive H atoms addition. DFT calculations show that the hydrogenation of MG is harder to be conquered than that of DMO. Either on SiO₂/Cu(111) or Cu(111), the energy gaps between TS5 and TS1 are nearly the same (0.42 eV ~0.45 eV) (from viii to ix in Supplementary Fig. 5). Structurally, DMO has two ester groups. When one of them is hydrogenated, the other serves as an electron-withdrawing group which can stabilize charged TS' through electron delocalization. Unfortunately, the CH₂OH group in MG lacks the ability to delocalize the negative charge upon ester hydrogenation. Thus, the rate determining step for the hydrogenation of DMO to EG is corresponding to the hydrogenation of MG.

The mechanism suggested by DFT calculations was verified by serial isotope-labeling experiments (Fig. 2b). The kinetic isotope effect (KIE) of Cu MPs@m-SiO₂ catalyst ($k_{\text{H}}/k_{\text{D}} = 3.5$) is about two times higher than that of Cu MPs catalyst ($k_{\text{H}}/k_{\text{D}} = 1.5$), indicating the different hydrogenation mechanisms on the two catalysts. As shown in Supplementary Fig. 5, not only the Cu–H but also the SiO–H are involved in the TS1 state as well as TS5 on SiO₂/Cu(111). It was expected that when hydrogen was replaced by deuterium, the vibrations of both Cu–D and SiO–D would contribute to the zero-point energy of TS', leading to a large KIE. It is particularly interesting that, when Cu MPs@m-SiO₂ was treated by a NaOH solution, Na⁺ ions pre-occupies the Cu–SiO sites so that the formation of SiO–H should be suppressed during the hydrogenation. As expected, the TOF for the NaOH-treated Cu MPs@m-SiO₂ catalyst was decreased dramatically to a similar level to that of uncoated Cu MPs, and the KIE was also dropped back to 1.6 (Supplementary Fig. 7). With the combination of DFT calculation and isotope-labelling experiments, we conclude that the Cu–O–SiO_x interface not only activates H₂ molecules in the heterolytic way to form Cu–H^{δ-} and SiO–H^{δ+}, but also facilitates the hydrogenation of ester by stabilizing the transition states.

Nanostructure engineering enriches the Cu–O–SiO_x interfaces.

As the promotional effect induced by the Cu–O–SiO_x interface, increasing Cu–O–SiO_x interfaces should lead to further enhanced catalytic efficiency. Thus, reducing the size of Cu particles to the nanoscale would amplify the interfacial effect. To create Cu–SiO₂ interface on Cu nanoparticles, Cu₂O nanoparticles were first prepared and coated by m-SiO₂ (Fig. 3a). The obtained Cu₂O@m-SiO₂ nanoparticles were then reduced under H₂ atmosphere to convert into Cu@m-SiO₂ nanoparticles (denoted as Cu-NP@m-SiO₂). Comprehensive characterizations by TEM, EDS, XRD (Fig. 3b–h), and N₂ adsorption/desorption isotherms (Supplementary Fig. 8) confirmed the core-shell structure of Cu-NP@m-SiO₂. As expected, the as-prepared Cu-NP@m-SiO₂ catalyst exhibited a much better catalytic performance in DMO hydrogenation than unmodified Cu NPs (Fig. 3i). With a liquid hourly space velocity (LHSV) of 2.4 h⁻¹, Cu-NP@m-SiO₂ exhibited both much higher DMO conversion (95.8%) and higher selectivity (93.3% to EG) at 200 °C. In contrast, when Cu NPs were used as the catalyst, only 35.6% of DMO was hydrogenated with 16.9% of selectivity to EG.

In term of Cu utilization, the core-shell overgrowth structure (Cu-NP@m-SiO₂) demonstrated above was not the ideal structure for practical applications because most of Cu atoms in Cu-NP@m-SiO₂ were not located on surface or Cu–O–SiO_x interfaces. In this regard, encapsulating ultra-small Cu nanoparticles in a porous SiO₂ matrix should be the most effective strategy to create highly active catalysts while maximizing the utilization of Cu. For this purpose, we chose copper phyllosilicate nanotubes as an alternative Cu precursor. Structurally, copper phyllosilicate has lamellar structure composed of alternate layers of SiO₄ tetrahedra and discontinuous layers of CuO₆ octahedra, in which Cu–O–SiO_x moieties are readily available (Supplementary Fig. 9)^{35–39}. By using a modified hydrothermal method, copper phyllosilicate nanotubes (Cu-PSNT) with sub-10 nm in diameter, 1–2 nm in wall thickness, and hundreds of nanometers in length were prepared (Fig. 4b). Both TEM and EDS analysis (Fig. 4c, Supplementary Fig. 10) confirmed the formation of metallic Cu nanoparticles which were embedded in SiO₂ matrix after the H₂ reduction. Some large Cu nanoparticles with size larger than 10 nm were also observed. Moreover, the BET analysis (Supplementary Fig. 11) revealed that the reduced Cu-PSNT had a BET surface area of 470.1 m² g⁻¹ and a pore volume of 1.47 cm³ g⁻¹.

To demonstrate the advantages of the reduced Cu-PSNT in catalysis, a Cu/SiO₂ catalyst (denoted as Cu/SiO₂-AE, Supplementary Fig. 12) was prepared by a reported ammonia-evaporation method for comparison^{38,40–42}. The Cu/SiO₂-AE catalyst represents the state-of-the-art Cu catalyst reported in the literature for the selective hydrogenation of DMO to EG^{29,43–45}. Although Cu nanoparticles in the reduced Cu-PSNT had an average size larger than that in the reduced Cu/SiO₂-AE (Supplementary Fig. 13), what particularly interesting is that, the reduced Cu-PSNT exhibited both much better activity and selectivity than the reduced Cu/SiO₂-AE (Supplementary Fig. 14). At 200 °C, the reduced Cu-PSNT showed 99.8% conversion of DMO as well as 97.9% selectivity to EG with a LHSV as high as 4.2 h⁻¹. In contrast, under the same reaction conditions, the reduced Cu/SiO₂-AE catalyst gave only 76.2% conversion of DMO and 68.9% selectivity to EG. It should be noted that, even after long time (24 h) catalysis, Cu nanoparticles in the reduced Cu/SiO₂-AE catalyst did not sinter much and were still smaller than those in the reduced Cu-PSNT catalyst (Supplementary Fig. 13).

The above catalysis comparison between Cu-PSNT and Cu/SiO₂-AE clearly indicated that the particle size of Cu was not the predominant factor to determine the catalytic performance. The enhanced performance should be attributed to the presence of more abundant Cu–O–SiO_x interfaces in the reduced Cu-PSNT than Cu/SiO₂-AE. In principle, the presence of abundant Cu–O–SiO_x interfaces should result in the presence of more Cu^{δ+} species in the reduced Cu-PSNT. While XPS measurements confirmed the reduction of Cu²⁺ in both reduced Cu-PSNT and Cu/SiO₂-AE composite (Supplementary Fig. 15), the Cu LMM XAES studies demonstrated that the Cu⁺/Cu⁰ ratios were much different in the two catalysts. Two overlapping peaks at 914.1 eV and 917.8 eV were ascribed to Cu⁺ and Cu⁰, respectively.^{28,46,47} The ratio of Cu⁺/Cu⁰ was 0.65 (Table S1) for the reduced Cu-PSNT, 1.2 times higher than that of the reduced Cu/SiO₂-AE catalyst (0.55). The high percentage of Cu⁺ confirmed the presence of more Cu–O–SiO_x interfaces in the reduced Cu-PSNT catalyst, consistent with our proposal that the Cu–O–SiO_x interface was the determining factor for the catalysis.

Maximizing both Cu–O–SiO_x interfaces and Cu utilization. It

should be noted that the simple reduction did not maximize the use of Cu due to the formation of some large Cu nanoparticles with size larger than 10 nm (Fig. 4c). There was still possibility to further improve the catalytic performance of Cu-PSNT if one could reduce the particle size of Cu nanoparticles during the H₂ treatment. To achieve this goal, our strategy was to encapsulate Cu-PSNT with a thin layer of m-SiO₂. The mesoporous layer SiO₂ was used to prevent the sintering of Cu nanoparticles during the H₂ treatment and also to create more Cu–O–SiO_x interfaces. The coating of the m-SiO₂ shell was carried out by hydrolysis of TEOS in the presence of CTAB (Fig. 4a, See Methods section)⁴⁸. In the as-obtained core-shell material (denoted as Cu-PSNT@m-SiO₂), the successful growth of a wormhole-like m-SiO₂ shell on Cu-PSNT was revealed by TEM analysis (Fig. 4d), and also confirmed by N₂ adsorption/desorption measurement (Supplementary Fig. 16). Compared with Cu-PSNT, the BET surface area of Cu-PSNT@m-SiO₂ was increased to 605.5 m² g⁻¹.

As expected, the SiO₂ coating on Cu-PSNT significantly prevented Cu nanoparticles from sintering during the H₂ treatment as revealed by TEM and XRD studies (Fig. 4e, Supplementary Fig. 17a). After 4-h H₂ treatment at 300 °C, the XRD and XPS results confirmed the reduction of Cu(II) in Cu-PSNT@m-SiO₂ into fine fcc Cu nanoparticles (Supplementary

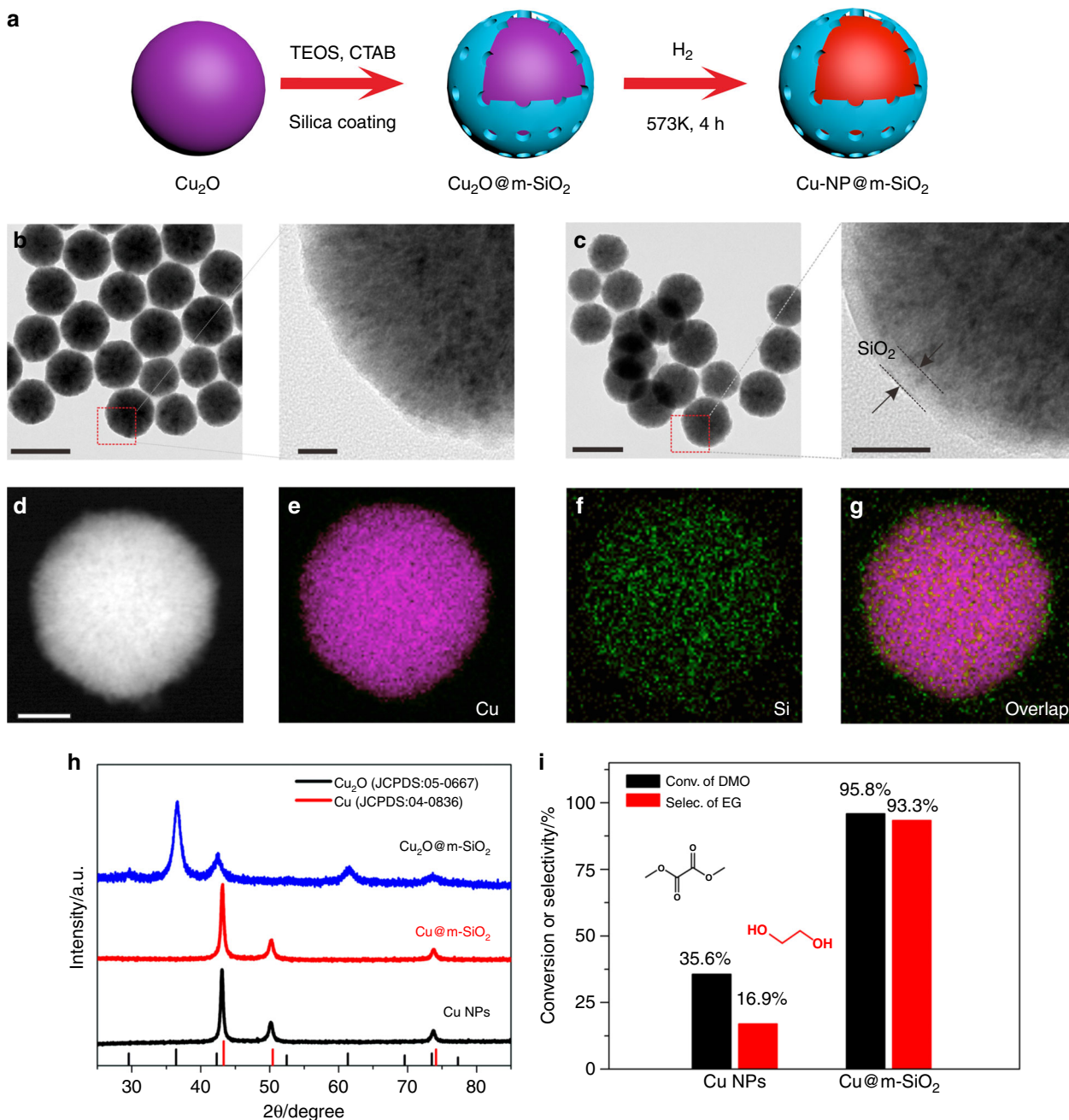


Fig. 3 Creating Cu–O–SiO_x interfaces on Cu nanoparticles. **a** Scheme for the synthesis of Cu@m-SiO₂; **b, c** TEM images of as-prepared Cu₂O nanoparticles and Cu₂O@m-SiO₂, respectively. **d–g** EDX mapping images of Cu₂O@m-SiO₂; **h** X-ray powder diffraction (XRD) pattern of Cu NPs, Cu₂O@m-SiO₂ and Cu@m-SiO₂; **i** Catalytic performance of Cu NPs and Cu@m-SiO₂ for the selective hydrogenation of DMO; Reaction conditions were as follows: H₂/DMO = 80 mol/mol, *P* (H₂) = 3.0 MPa, *T* = 200 °C, LHSV = 2.4 h⁻¹. Scale bars in **b** (left) and **c** (left) are 200 nm. Scale bars in **b** (right) and **c** (right) are 20 nm. Scale bar in **d** is 50 nm

Figs. 15 and 17a). The yielded Cu nanoparticles were even too small to be clearly detected by TEM and STEM (Fig. 4e and Supplementary Fig. 17b) due to the limited electronic contrast between Cu and SiO₂. No formation of large Cu nanoparticles with size larger than 2 nm was observed in the reduced Cu-PSNT@m-SiO₂ catalyst, dramatically different from the reduced Cu-PSNT. As determined by ICP-AES, the Cu content in Cu-PSNT@m-SiO₂ was as high as 20.5 wt% (Supplementary Table 2). More importantly, the ratio of Cu⁺/Cu⁰ demonstrated by Cu LMM XAES spectra is 0.99 (Supplementary Fig. 15 and Supplementary Table 1), 1.5 and 1.8 times higher than those of Cu-PSNT and Cu/SiO₂-AE catalysts. These results suggested

that Cu in reduced Cu-PSNT@m-SiO₂ were present mainly in the form of ultrafine nanoparticles confined in the SiO₂ matrix. The confinement of fine Cu nanoparticles in porous SiO₂ was expected to create abundant Cu–O–SiO_x interfaces to boost the hydrogenation. In situ FT-IR measurements over the reduced Cu-PSNT@m-SiO₂ catalyst under D₂ atmosphere revealed the formation of SiO–D (Supplementary Fig. 18), further confirming the heterolytic activation pathway of D₂ over the Cu–O–SiO_x interfaces.

As compared to the reduced Cu-PSNT catalyst with the same amount of Cu, the catalytic performance of the reduced Cu-PSNT@m-SiO₂ catalyst was greatly enhanced in both activity

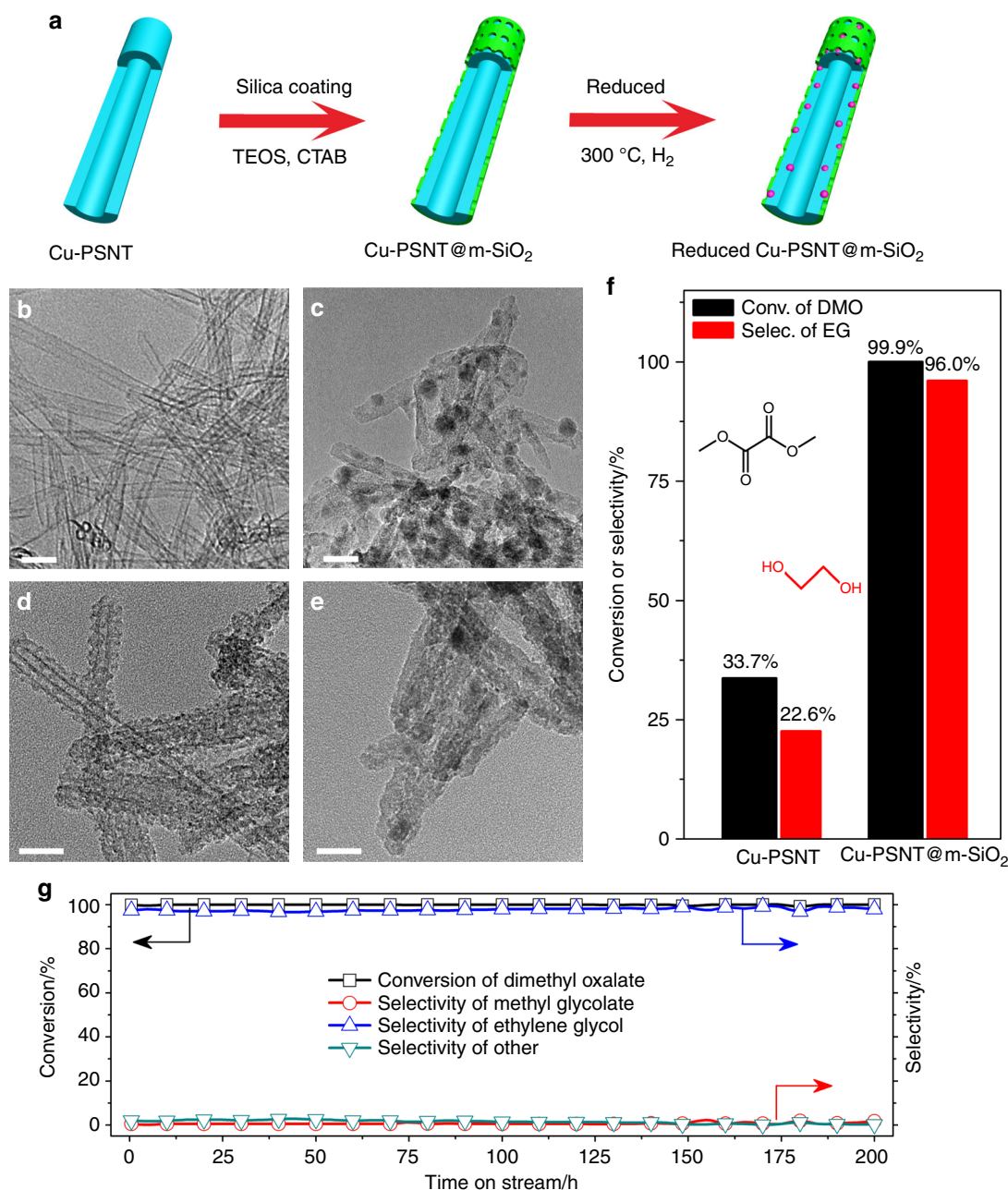


Fig. 4 Confined growth strategy for maximizing Cu-O-SiO_x interface. **a** Illustration of the synthetic strategy for the preparation of Cu-PSNT@m-SiO₂; **b-e** TEM image of as-prepared Cu-PSNT, reduced Cu-PSNT, Cu-PSNT@m-SiO₂ and reduced Cu-PSNT@m-SiO₂, respectively; **f** Catalytic performance of reduced Cu-PSNT and reduced Cu-PSNT@m-SiO₂ for the selective hydrogenation of DMO to EG (LHSV = 7.8 h⁻¹); **g** Catalytic performance of reduced Cu-PSNT@m-SiO₂ catalyst as a function of time-on-stream (LHSV = 2.0 h⁻¹). Reaction conditions were as follows: H₂/DMO = 80 mol/mol, P (H₂) = 3.0 MPa, T = 200 °C. Scale bars are 20 nm for (b-e)

and selectivity for DMO hydrogenation to EG. As shown in Fig. 4f, a nearly 100 % conversion of DMO and a high selectivity of 96.0% to EG were achieved over the reduced Cu-PSNT@m-SiO₂ catalyst even at a LHSV as high as 7.8 h⁻¹ at 200 °C. Under the same catalytic conditions (high LHSV), the reduced Cu-PSNT only gave 33.7% conversion of DMO and 22.6% selectivity to EG. The TOF (Supplementary Table 2) of the reduced Cu-PSNT@m-SiO₂ catalyst (40.62 h⁻¹) was much higher than that of the reduced Cu-PSNT (23.08 h⁻¹) or Cu/SiO₂-AE (10.21 h⁻¹) catalyst. More importantly, after catalysis studies at different LHSVs, no formation of large Cu nanoparticles caused by sintering was observed over the reduced Cu-PSNT@m-SiO₂ catalyst (Supplementary Fig. 19). The reduced Cu-PSNT@m-SiO₂

also displayed excellent stability in the time-on-stream experiment (Fig. 4g). No decay in the activity and stability of the reduced Cu-PSNT@m-SiO₂ catalyst was observed even after the 200 h time-on-stream (LHSV = 2.0 h⁻¹) experiment. Additionally, the reduced Cu-PSNT@m-SiO₂ also displayed excellent stability in ultra-high temperature and ultra-high LHSV (Supplementary Fig. 20). At 280 °C, the reduced Cu-PSNT@m-SiO₂ exhibited ~95% conversion of DMO as well as ~90% selectivity of EG with a LHSV as high as 300 h⁻¹ during the long time (16 h) catalysis. To the best of our knowledge, the catalytic activity of the reduced Cu-PSNT@m-SiO₂ showed the best performance among reported copper-based catalysts for ester hydrogenation (Supplementary Table 3).

Although SiO₂ has been long considered as an inert support to create active metal-support interface for promoting catalysis, we demonstrate in this work that Cu–O–SiO_x is a very active interface in selective hydrogenation of DMO to EG. The activity of silica-coated Cu catalysts with Cu–O–SiO_x interfaces in selective hydrogenation of DMO is approximately 80 times higher than that on pristine Cu at the temperature between 200 and 240 °C. With the combination of DFT calculations and isotope-labelling experiments, the catalytic mechanism on Cu–O–SiO_x interface has been well clarified. The existence of Cu–H^{δ-} and SiO–H^{δ+} at Cu–O–SiO_x interfaces would facilitate the hydrogenation of ester by stabilizing the hydrogenation transition states. Based on this mechanism, we developed a confined growth strategy to maximize Cu–O–SiO_x interfaces and Cu utilization. By coating copper phyllosilicate nanotubes with mesoporous silica followed by hydrogen reduction, a practical Cu nanocatalyst was produced and possessed abundant Cu–O–SiO_x interfaces and thus exhibited the best performance in the hydrogenation of DMO to EG among all reported Cu catalysts. We envision that the discovery of the active Cu–O–SiO_x interface for promoting catalysis in this work will lead us to revisit the support effects of SiO₂ and create practical SiO₂-supported metal nanocatalysts with enhanced catalytic activity, selectivity, and durability.

Methods

Materials. Colloidal silica (Ludox-HS 40, SiO₂ 40 wt % aqueous solution), methanol and tetraethyl orthosilicate were purchased from Alfa Aesar Chemical Reagent Co. Ltd. (Tianjin, China). Cu(NO₃)₂·3H₂O, DMO, CuCl₂·2H₂O, ammonium chloride, ethanol, N-hexadecyltrimethylammonium bromide and ammonia aqueous solution (25%–28%) were purchased from Sinopharm Chemical Reagent Co. Ltd. (Shanghai, China). Cu powder was purchased from Tianjin Guangfu Fine Chemical Co., Ltd. Deuterium gas (99.999%) was purchased from Chengdu Keyuan Gas Co. Ltd. All reagents were used as received without further purification. Water used in the studies was ultrapure water (Millipore, ≥18 MΩ cm).

Synthesis of cuprous oxide nanoparticles (Cu₂O NPs). Cu₂O NPs were prepared by using the high-temperature ploy-mediated methods reported by Zeng⁴⁹. In a typical synthesis of Cu₂O NPs, 0.5 mmol of Cu(NO₃)₂·3H₂O and 1.0 g of PVP were dissolved in 10 mL of DEG. The mixed solution was heated from room temperature to 190 °C in 0.5 h under argon atmosphere. The products were collected by centrifugation and washed with ethanol for several times. Finally, the products were dispersed in ethanol for further use.

Synthesis of Cu₂O NPs coated with mesoporous silica. Cu₂O@m-SiO₂ were prepared by using the modified method reported by Fang⁵⁰. In a typical synthesis of Cu₂O@m-SiO₂, 0.2 g of Cu₂O NPs and 1 g of CTAB were added into 200 mL water in flask under argon atmosphere and then transferred to a 45 °C water bath. Then, 5 mL of ethanol and 0.4 mL of TEOS were added into above mixture and stirred for another 30 min. The products were collected by centrifugation and washed with ethanol several times. The method of extraction was used to remove CTAB from the products. Briefly, the products were dispersed in 100 mL of acetone and refluxed at 80 °C for 8 h. The extraction was repeated three times to fully remove CTAB. Finally, the products were collected by centrifugation and washed with ethanol several times.

Synthesis of copper phyllosilicate nanotubes. Copper phyllosilicate nanotubes (Cu-PSNT) were prepared by a hydrothermal method. Typically, 6.5 mmol of copper (II) salt (CuCl₂·2H₂O or Cu(NO₃)₂·3H₂O) and 26 mmol of NH₄Cl were dissolved in 60 mL water, into which 5 mL of NH₃·H₂O was added to form a blue solution. Then, 1 g of silica colloidal (SiO₂ 40 wt %) was added into above solution. Subsequently, the mixture was transferred into 100 mL capacity Teflon-lined stainless steel autoclave and then the autoclave was put in an oven at 200 °C for 48 h. The blue products were collected by centrifugation and washed with water for several times. Finally, the blue products were dried in a vacuum oven at 60 °C for 12 h.

Synthesis of Cu-PSNT coated with mesoporous silica. Cu-PSNT@m-SiO₂ was prepared using the modified method reported by Fang⁵⁰. For a typical synthesis of Cu-PSNT@m-SiO₂, 0.6 g of copper phyllosilicate nanotubes was dispersed into 200 mL water containing 1 g of CTAB in the flask. The mixture was transferred to a 45 °C water bath and then ethanol (5 mL) and TEOS (2 mL) were added. After 30 min, the products were collected by centrifugation and washed with ethanol several

times. Subsequently, the products were dried in a vacuum oven at 60 °C for 12 h. Calcination was used to remove CTAB and the products were heated to 500 °C (2 °C/min) for 2 h in air.

Synthesis of the Cu/SiO₂-AE catalyst. Cu/SiO₂-AE was prepared by ammonia evaporation method³⁸. The ammonia evaporation method was described as follows: 3.05 g of Cu(NO₃)₂·3H₂O was dissolved in a mixture of ultrapure water (75 mL) and ammonia aqueous (5 mL). Then, 20 g of silica colloidal (SiO₂ 40 wt %) was added into above copper ammonia complex solution. Subsequently, the mixed solution was heated in an 85 °C water bath to evaporate ammonia. As the process continues, the pH value of the mixture decreased slowly. When the pH value decreased below 7.0, the products were collected by centrifugation and washed with water for several times. Finally, the products were dried in an oven at 60 °C for 12 h and then were heated to 500 °C (2 °C per min) for 2 h in air.

Characterizations. Transmission electron microscopy (TEM) images were taken on a TECNAI F-30 high-resolution transmission electron microscope operating at 300 kV. The conventional and in situ X-ray powder diffraction (XRD) were performed with PANalytical X'pert PRO diffractometer using Cu K_α radiation ($\lambda = 0.15418$ nm), operating at 40 kV and 30 mA. For the in situ XRD measurement, the samples were put in an in situ chamber and 5%H₂-95%N₂ mixture gas was introduced to the system at a flow rate of 50 mL per min. Then, the sample was heated to 573 K (2 °C per min) for 4 h. When the temperature of sample cooled to room temperature, the XRD patterns were collected. N₂ adsorption-desorption measurements were carried on a Micrometrics ASAP 2020 system. Pore size distributions were calculated from desorption branch by the Barrett-Joyner-Halenda (BJH) method. The total pore volume depended on the desorption N₂. X-ray photoelectron spectroscopy (XPS) and X-ray induced Auger electron spectroscopy (XAES) were obtained using a PHI Quantum 2000 Scanning ESCA Microprobe instrument (physical Electronics) equipped with an Al K_α X-ray source ($h\nu = 1486.6$ eV) and binding energies referenced to C 1 s (284.8 eV). For quasi-in situ XPS measurement, the samples were treated with 5%H₂-95%N₂ (573K-4 h) in an in situ chamber, and then evacuated to obtain a high vacuum environment. Finally, the reduced samples were transferred from in situ chamber to testing chamber under vacuum conditions. The precise copper content of sample was determined by the inductively coupled plasma atomic emission spectroscopy (ICP-AES, Baird PS-4). The copper dispersions of the samples were measured by N₂O titration on a Micromeritics Autochem II 2920 apparatus with a TCD. Typical steps as follows: (1) Samples were reduced in a 5%H₂-95%N₂ atmosphere (50 mL per min) at 573 K for 4 h (hydrogen consumption was denoted as A₁) and then cooled down to 333 K in argon atmosphere. (2) The surface copper atoms were oxidized to Cu₂O by N₂O (30 mL/min) for 0.5 h and then the argon was introduced to the system for 0.5 h to remove the N₂O. (3) The reduction of surface Cu₂O to copper was carried out by a 5%H₂-95%N₂ mixture gas (50 mL per min) at 773 K for 2 h (hydrogen consumption was denoted as A₂). The dispersion (D) of copper was calculated by $D = (2A_2/A_1) \times 100\%$.

Catalytic performance tests. The catalytic performance for DMO hydrogenation was evaluated by using a fixed-bed microreactor. Typically, 200 mg of the catalyst was placed in the middle of the quartz tube and packed with quartz powders in the top side. The quartz tube was then loaded into the stainless steel tubular reactor. The catalyst was reduced under a 5%H₂-95%N₂ flow (50 mL per min) at 573 K (2 °C per min) for 4 h. The catalyst was cooled to desired reaction temperature (473 K). Subsequently, 10 wt % DMO in methanol and H₂ were fed into the reactor at a H₂/DMO molar ratio of 80 under a system pressure of 3.0 MPa. The liquid hourly space velocity of DMO was varied by changing the amount of feedstock. The outlet stream was sampled by an automatic Valco 6-ports valve system and analyzed by an online gas chromatograph (GC-9790, FuLi) with a flame ionization detector and a KB-Wax capillary column (30 m × 0.45 mm × 0.85 μm) at intervals of 0.5 h.

Computational details. DFT calculations are carried out by using the Vienna ab initio simulation package (VASP)^{51,52}. Exchange and correlation were treated within the Perdew-Burke-Ernzerhof (PBE) generalized gradient approximation (GGA)⁴³. The valence electrons are described by plane wave basis sets with a cut off energy of 400 eV, and the core electrons are replaced by the projector augmented wave pseudopotentials^{53,54}. For a clean Cu(111) surface, a (5 × 3) supercell with five layer slabs was used, which for the SiO₂/Cu(111), the Cu(111) substrate was extended into the (8 × 4) structure. During structural optimization, the bottom two layer slabs were fixed at a bulk truncated position, while the surface layers and the adsorbates were fully relaxed. For all of the calculations, the vacuum regions between the slabs were more than 10 Å, and Monkhorst-Pack k-point sampling with approximately 0.05 × 2π Å⁻¹ spacing in a reciprocal lattice was utilized. The minimum energy reaction pathways were calculated using the nudged elastic band method. The final transition state structures were refined using a quasi-Newton algorithm until the Hellman-Feynman forces on each ion were lower than 0.03 eV Å⁻¹. The adsorption energies (ΔE_{ads}) were calculated using Eq. 1, in which $E_{\text{ad/surf}}$, E_{ads} , and E_{surf} were the total energies of the optimized adsorbate/surface system, the adsorbate in the gas phase, and the surface respectively. For the DMO

hydrogenation, we assumed that there already existed four adsorbed H atoms on the Cu(111) surface and SiO₂/Cu(111) interface.

$$\Delta E_{\text{ads}} = E_{\text{ad/surf}} - E_{\text{ad}} - E_{\text{surf}} \quad (1)$$

Data availability. The data that support the findings of this study are available from the corresponding author upon reasonable request.

Received: 10 December 2017 Accepted: 18 July 2018

Published online: 22 August 2018

References

- Fu, Q. et al. Interface-confined ferrous centers for catalytic oxidation. *Science* **875**, 26–29 (2010).
- Qiao, B. et al. Single-atom catalysis of CO oxidation using Pt₁/FeO_x. *Nat. Chem.* **3**, 634–641 (2011).
- Chen, G. X. et al. Interfacial effects in iron-nickel hydroxide-platinum nanoparticles enhance catalytic oxidation. *Science* **344**, 495–499 (2014).
- Fu, Q., Yang, F. & Bao, X. H. Interface-confined oxide nanostructures for catalytic oxidation reactions. *Acc. Chem. Res.* **46**, 1692–1701 (2013).
- Park, J. B. et al. High catalytic activity of Au/CeO_x/TiO₂(110) controlled by the nature of the mixed-metal oxide at the nanometer level. *Proc. Natl Acad. Sci.* **106**, 4975–4980 (2009).
- Rodriguez, J. A. et al. Activity of CeO_x and TiO_x nanoparticles grown on Au (111) in the water-gas shift reaction. *Science* **318**, 1757–1760 (2007).
- Fu, Q., Saltsburg, H. & Flytzani-Stephanopoulos, M. Active nonmetallic Au and Pt species on ceria-based water-gas shift catalysts. *Science* **301**, 935–938 (2003).
- Subbaraman, R. et al. Trends in activity for the water electrolyzer reactions on 3d M(Ni,Co,Fe,Mn) hydro(oxy)oxide catalysts. *Nat. Mater.* **11**, 550–557 (2012).
- Subbaraman, R. et al. Enhancing hydrogen evolution activity in water splitting by tailoring Li⁺-Ni(OH)₂-Pt interfaces. *Science* **334**, 1256–1260 (2011).
- Danilovic, N. et al. Enhancing the alkaline hydrogen evolution reaction activity through the bifunctionality of Ni(OH)₂/metal catalysts. *Angew. Chem. Int. Ed.* **124**, 12663–12666 (2012).
- Strmcnik, D. et al. Improving the hydrogen oxidation reaction rate by promotion of hydroxyl adsorption. *Nat. Chem.* **5**, 300–306 (2013).
- Tauster, S. J., Fung, S. C. & Garten, R. L. Strong interactions in supported-metal catalysts. *Science* **211**, 1121–1125 (1981).
- Tauster, S. J. Strong metal-support interactions. *Acc. Chem. Res.* **20**, 389–394 (1987).
- Tauster, S. J. et al. Strong metal-support interactions. Group 8 noble metals supported on titanium dioxide. *J. Am. Chem. Soc.* **100**, 170–175 (1978).
- Matsubu, J. C. et al. Adsorbate-mediated strong metal-support interactions in oxide-supported Rh catalysts. *Nat. Chem.* **9**, 120–127 (2017).
- Rodriguez, J. A. et al. Ceria-based model catalysts: fundamental studies on the importance of the metal-ceria interface in CO oxidation, the water-gas shift, CO₂ hydrogenation, and methane and alcohol reforming. *Chem. Soc. Rev.* **46**, 1824–1841 (2017).
- Graciani, J. et al. Highly active copper-ceria and copper-ceria-titania catalysts for methanol synthesis from CO₂. *Science* **345**, 546–550 (2014).
- Zhang, Q. et al. Core-shell nanostructured catalysts. *Acc. Chem. Res.* **46**, 1816–1824 (2013).
- Zaera, F. Nanostructured materials for applications in heterogeneous catalysis. *Chem. Soc. Rev.* **42**, 2746–2762 (2013).
- Joo, S. H. et al. Thermally stable Pt/mesoporous silica core-shell nanocatalysts for high-temperature reactions. *Nat. Mater.* **8**, 126–131 (2009).
- Dai, Y. Q. et al. A sinter-resistant catalytic system based on platinum nanoparticles supported on TiO₂ nanofibers and covered by porous silica. *Angew. Chem. Int. Ed.* **49**, 8165–8168 (2010).
- Hansen, T. W. et al. Sintering of catalytic nanoparticles: particle migration or Ostwald ripening? *Acc. Chem. Res.* **46**, 1720–1730 (2013).
- Wu, S. H., Mou, C. Y. & Lin, H. P. Synthesis of mesoporous silica nanoparticles. *Chem. Soc. Rev.* **42**, 3862–3875 (2013).
- Gawande, M. B. et al. Core-shell nanoparticles: synthesis and applications in catalysis and electrocatalysis. *Chem. Soc. Rev.* **44**, 7540–7590 (2015).
- Yamada, Y. et al. Nanocrystal bilayer for tandem catalysis. *Nat. Chem.* **3**, 372–376 (2011).
- Berne, B. J. et al. Nitriles at silica interfaces resemble supported lipid bilayers. *Acc. Chem. Res.* **49**, 1605–1613 (2016).
- Yue, H. R. et al. A copper-phyllisilicate core-sheath nanoreactor for carbon-oxygen hydrogenolysis reactions. *Nat. Commun.* **4**, 2339 (2013).
- Gong, J. L. et al. Synthesis of ethanol via syngas on Cu/SiO₂ catalysts with balanced Cu⁰-Cu⁺ sites. *J. Am. Chem. Soc.* **134**, 13922–13925 (2012).
- Yue, H. R. et al. Ethylene glycol: properties, synthesis, and applications. *Chem. Soc. Rev.* **41**, 4218–4244 (2012).
- Löffler, D. et al. Growth and structure of crystalline silica sheet on Ru (0001). *Phys. Rev. Lett.* **105**, 146104 (2010).
- Chen, M. S., Santra, A. K. & Goodman, D. W. Structure of thin SiO₂ films grown on Mo (112). *Phys. Rev. B* **69**, 155404 (2004).
- Shaikhutdinov, S. & Freund, H. J. Ultrathin silica films on metals: the long and winding road to understanding the atomic structure. *Acc. Chem. Res.* **25**, 49–67 (2013).
- Konda, S. S. M. et al. Computational insights into the role of metal and acid sites in bifunctional metal/zeolite catalysts: a case study of acetone hydrogenation to 2-propanol and subsequent dehydration to propene. *ACS Catal.* **6**, 123–133 (2015).
- Sinha, N. K. & Neurock, M. A first principles analysis of the hydrogenation of C₁-C₄ aldehydes and ketones over Ru(0001). *J. Catal.* **295**, 31–44 (2012).
- Toupance, T., Kermarec, M. & Louis, C. Metal particle size in silica-supported copper catalysts. Influence of the conditions of preparation and of thermal pretreatments. *J. Phys. Chem. B* **104**, 965–972 (2000).
- Wang, Y. Q., et al. One-pot synthesis of nanotube-based hierarchical copper silicate hollow spheres. *Chem. Commun.* **0**, 6555–6557 (2008).
- Wang, X. et al. Thermally stable silicate nanotubes. *Angew. Chem. Int. Ed.* **43**, 2017–2020 (2004).
- Chen, L. F. et al. Cu/SiO₂ catalysts prepared by the ammonia-evaporation method: texture, structure, and catalytic performance in hydrogenation of dimethyl oxalate to ethylene glycol. *J. Catal.* **257**, 172–180 (2008).
- Toupance, T. et al. Conditions of formation of copper phyllosilicates in silica-supported copper catalysts prepared by selective adsorption. *J. Phys. Chem. B* **106**, 2277–2286 (2002).
- Zhao, S. et al. Chemoselective synthesis of ethanol via hydrogenation of dimethyl oxalate on Cu/SiO₂: Enhanced stability with boron dopant. *J. Catal.* **297**, 142–150 (2013).
- Wang, Z. Q. et al. High-performance and long-lived Cu/SiO₂ nanocatalyst for CO₂ hydrogenation. *ACS Catal.* **5**, 4255–4259 (2015).
- Ye, R. P. et al. A new low-cost and effective method for enhancing the catalytic performance of Cu-SiO₂ catalysts for the synthesis of ethylene glycol via the vapor-phase hydrogenation of dimethyl oxalate by coating the catalysts with dextrin. *J. Catal.* **350**, 122–132 (2017).
- Yue, H. R., Ma, X. B. & Gong, J. L. An alternative synthetic approach for efficient catalytic conversion of syngas to ethanol. *Acc. Chem. Res.* **47**, 1483–1492 (2014).
- He, Z. et al. Effect of boric oxide doping on the stability and activity of a Cu-SiO₂ catalyst for vapor-phase hydrogenation of dimethyl oxalate to ethylene glycol. *J. Catal.* **277**, 54–63 (2011).
- Huang, Y. et al. Silver-modulated SiO₂-supported copper catalysts for selective hydrogenation of dimethyl oxalate to ethylene glycol. *J. Catal.* **307**, 74–83 (2013).
- Yin, A. Y. et al. The nature of active copper species in Cu-HMS catalyst for hydrogenation of dimethyl oxalate to ethylene glycol: new insights on the synergetic effect between Cu and Cu⁺. *J. Phys. Chem. C* **113**, 11003–11013 (2009).
- Chusuei, C. C., Brookshier, M. A. & Goodman, D. W. Correlation of relative X-ray photoelectron spectroscopy shake-up intensity with CuO particle size. *Langmuir* **15**, 2806–2808 (1999).
- Fang, W. J. et al. Photo- and pH-triggered release of anticancer drugs from mesoporous silica-coated Pd@Ag nanoparticles. *Adv. Funct. Mater.* **22**, 842–848 (2012).
- Xiong, S. L. & Zeng, H. C. Serial ionic exchange for the synthesis of multishelled copper sulfide hollow spheres. *Angew. Chem. Int. Ed.* **51**, 949–952 (2012).
- Fang, W. J. et al. Pd nanosheet-covered hollow mesoporous silica nanoparticles as a platform for the chemo-photothermal treatment of cancer cells. *Small* **8**, 3816–3822 (2012).
- Kresse, G. & Furthmüller, J. Efficient iterative schemes for ab initio total-energy calculations using a plane-wave basis set. *Phys. Rev. B* **54**, 11169–11186 (1996).
- Kresse, G. & Furthmüller, J. Efficiency of ab initio total energy calculations for metals and semiconductors using a plane-wave basis set. *Comput. Mater. Sci.* **6**, 15–50 (1996).
- Blöchl, P. E. Projector augmented-wave method. *Phys. Rev. B* **50**, 17953–17979 (1994).
- Kresse, G. & Joubert, D. From ultrasoft pseudopotentials to the projector augmented-wave method. *Phys. Rev. B* **59**, 1758–1775 (1999).

Acknowledgements

We thank the National Key R&D Program of China (2017YFA0207302, 2017YFA0207303, 2017YFA0206801), the NNSF of China (21731005, 21420102001, 21721001, 21333008, 21373167, 21573178), and the Fundamental Research Funds for the Central Universities (20720160046) for financial support.

Author contributions

C. X. and G. C. conceived and carried out experiments, analyzed data, and wrote the paper. C. X. and G. C. contributed equally to this work. N. Z. designed the study, supervised the project, analyzed data, and wrote the paper. P. L., Y. Z. and G. F. carried out the density functional calculations, analyzed result and wrote the paper. L. G. carried out the STEM measurements. X. D. and Y. Y. carried out catalytic tests. All the authors contributed to the paper revision.

Additional information

Supplementary Information accompanies this paper at <https://doi.org/10.1038/s41467-018-05757-6>.

Competing interests: The authors declare no competing interests.

Reprints and permission information is available online at <http://npg.nature.com/reprintsandpermissions/>

Publisher's note: Springer Nature remains neutral with regard to jurisdictional claims in published maps and institutional affiliations.



Open Access This article is licensed under a Creative Commons Attribution 4.0 International License, which permits use, sharing, adaptation, distribution and reproduction in any medium or format, as long as you give appropriate credit to the original author(s) and the source, provide a link to the Creative Commons license, and indicate if changes were made. The images or other third party material in this article are included in the article's Creative Commons license, unless indicated otherwise in a credit line to the material. If material is not included in the article's Creative Commons license and your intended use is not permitted by statutory regulation or exceeds the permitted use, you will need to obtain permission directly from the copyright holder. To view a copy of this license, visit <http://creativecommons.org/licenses/by/4.0/>.

© The Author(s) 2018